SOLUTION MINING RESEARCH INSTITUTE
105 Apple Valley Circle
Clarks Summit, PA 18411, USA

Telephone: +1 570-585-8092
Fax: +1 570-585-8091
www.solutionmining.org

Technical Conference Paper

THE EFFECT OF SMALL DEVIATORIC STRESSES ON CAVERN CREEP BEHAVIOR

Pierre Bérest, Ecole Polytechnique, Palaiseau, France
Benoît Brouard, Brouard Consulting, Paris, France
Mehdi Karimi-Jafari, Sofregaz, Paris, France

SMRI Fall 2008 Technical Conference
13-14 October 2008
Galveston, Texas

THE EFFECT OF SMALL DEVIATORIC STRESSES ON CAVERN CREEP BEHAVIOR

Bérest Pierre
LMS, Ecole Polytechnique – Route de Saclay, 91128 Palaiseau, France

Brouard Benoit
Brouard Consulting – 101 rue du Temple, 75003 Paris, France

Karimi-Jafari Mehdi
Sofregaz – 92/98 bd Victor Hugo, 92115 Clichy, France

SUMMARY

The rate of salt creep under small deviatoric stresses ($\sigma < 5$ MPa) is likely to be much faster than what usually is inferred from laboratory tests performed under higher mechanical loadings. Potential consequences regarding cavern-closure prediction are significant.

1. SALT CREEP BEHAVIOR UNDER SMALL DEVIATORIC STRESSES

1.1. Micro-mechanisms governing salt creep

Hunsche (1984), Munson and Dawson (1984), Langer (1984), and Blum and Fleischman (1988) have discussed the micro-mechanisms that govern salt creep. Langer (1984) states that:

> *Reliable extrapolation of the creep equations over long period of time and at low deformation rates can only be carried out on the basis of deformation mechanisms. The construction of a deformation-mechanism map is an essential preliminary.*

Such a map (adapted from Munson and Dawson, 1984) is presented in Figure 1. The governing creep-mechanism is indicated for each domain of the Temperature-Deviatoric Stress plane. Two rectangles also are drawn; the $[0-120°C]\times[5-20MPa]$ rectangle is the domain in which laboratory tests generally are performed. As will be seen, the $[0-120°C]\times[0-5MPa]$ rectangle is the domain of temperature and deviatoric stress *actually* experienced in the vicinity of salt caverns during most of their lifetime (gas storage caverns, which experience large pressure changes, are an outstanding exception). Except for the upper part of the first rectangle, in which dislocation creep is the dominant mechanism, the micro-mechanism that governs creep in these two rectangles is poorly known. However, Spiers et al. (1990) suggested that, in the low stress range, pressure solution was an important mechanism (see Section 1.3).

In other words, prediction of the mechanical behavior of a cavern is based on empirical data. Furthermore, as tests are performed in the 5-20 MPa deviatoric stress range, empirical creep laws inferred from laboratory testing must be extrapolated to the 0-5 MPa deviatoric stress range (the range of primary interest when considering cavern behavior), for which no or few actual data are available.

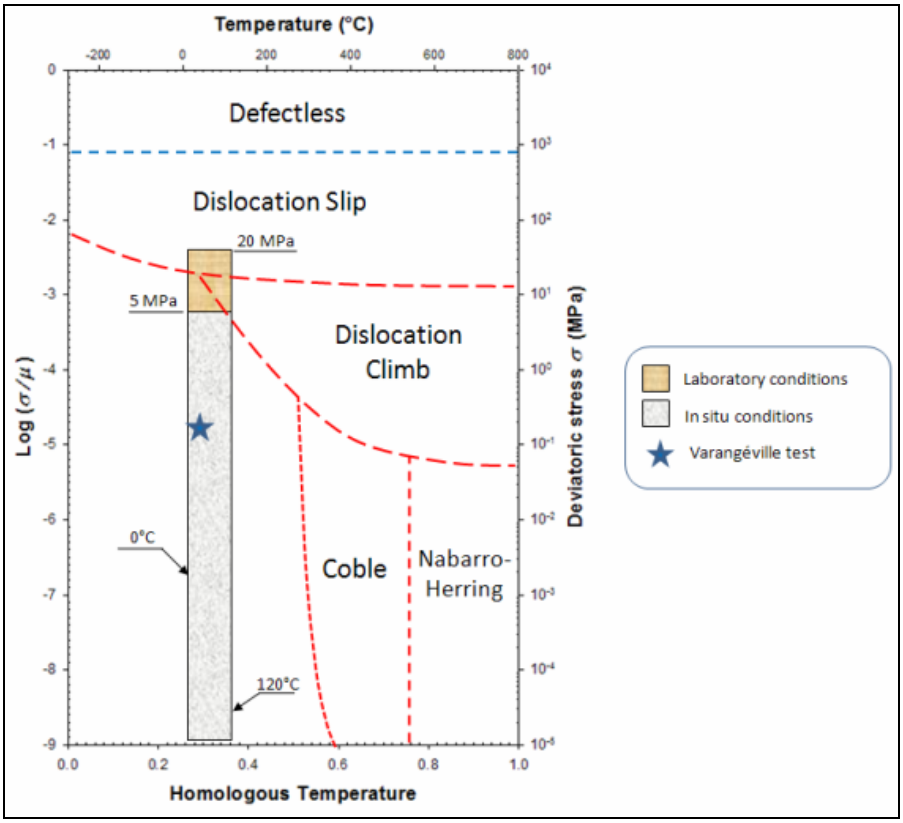

Figure 1. Mechanism Map (after Munson and Dawson, 1984). Stress and temperature conditions during the test described in Section 15 are represented by a star.

1.2. Norton-Hoff Law and small deviatoric stresses

Steady-state creep rates, as observed during laboratory tests performed in the 5- to 20-MPa range, often are fitted against the deviatoric stress. In the range of temperatures experienced in most salt caverns, the Norton-Hoff law captures the main features of the steady-state behavior of salt:

$$\dot{\varepsilon} = A\exp\left(-\frac{Q}{RT}\right)\sigma^n \tag{1}$$

where n belongs to the range n = 3-6. When the deviatoric stress is $\sigma = 10$ MPa, a typical steady-state strain rate is $\dot{\varepsilon} = 10^{-10}$ s^{-1} $\left(3\times10^{-3}\ \text{yr}^{-1}\right)$. When n = 3 is allowed, the (extrapolated) steady-state strain rate is $\dot{\varepsilon} = 10^{-13}$ s^{-1} when the deviatoric stress is $\sigma = 1$ MPa; it is $\dot{\varepsilon} = 10^{-16}$ s^{-1} when the deviatoric stress is $\sigma = 0.1$ MPa. This last strain rate is exceedingly slow: after a period lasting 300,000 years, the cumulated strain is $\varepsilon = 10^{-3}$. Such slow strain rates cannot be observed in the laboratory.

1.3. Norton-Hoff Law and cavern convergence computations

Equation (1) holds for creep tests performed on cylindrical samples. It needs to be generalized to 3D situations:

$$\dot{\varepsilon}_{ij} = \frac{1+\nu}{E}\dot{\sigma}_{ij} - \frac{\nu}{E}\dot{\sigma}_{kk}\delta_{ij} + \frac{3}{2}A^*\left(\sqrt{3J_2}\right)^{n-1}s_{ij} \tag{2}$$

where $A^* = A\exp(-Q/RT)$; s_{ij} is the deviatoric stress tensor and $J_2 = s_{ij}s_{ji}/2$ is the second invariant of the deviatoric stress tensor. It is important to assess the consequences of this with regard to the mechanical behavior of salt caverns. Consider the case of an idealized spherical cavern of radius *a* in an infinite elasto-visco-plastic medium. The geostatic pressure at cavern depth is P_∞. At time $t = 0$, the cavern is submitted to an internal pressure $P_c < P_\infty$, which, later (*t > 0*), is kept constant. In a 1000-m deep brine-filled cavern, $P_\infty - P_c = 10$ MPa is typical. After the initial rapid pressure change, the cavern experiences a transient phase during which the deviatoric stresses decrease, and, after a (long) period of time, steady state is reached. The steady-state volume-loss rate and the steady-state deviatoric stress distribution can be computed easily (see Appendix A):

$$\left.\frac{\dot{V}}{V}\right|_{SS}^{NH} = -\frac{3}{2}A^*\left[\frac{3}{2n}\left(P_\infty - P_c\right)\right]^n \tag{3}$$

$$\left.\sqrt{3J_2}\right|_{SS}^{NH} = \frac{3}{2n}\left(P_\infty - P_c\right)\left(\frac{a}{r}\right)^{3/n} \tag{4}$$

Formula (4) links the deviatoric stress ($\sqrt{3J_2}$) to the pressure difference ($P_\infty - P_c$) and to the distance to the cavern centre (r). It is interesting to compare this "steady-state" stress distribution to the "elastic" stress distribution that is observed immediately after the beginning of the transient phase, when the internal pressure $P_c < P_\infty$ is applied:

$$\left.\sqrt{3J_2}\right|_{SS}^{EL} = \frac{3}{2}\left(P_\infty - P_c\right)\left(\frac{a}{r}\right)^3 \tag{5}$$

First, the perturbation to the natural isotropic state of stress penetrates much deeper inside the rock mass for the steady-state solution. For example, when $n = 3$, at a distance $r = 2a$ from the cavern centre, the "elastic" deviatoric stress is divided by 8 (compared to its value at *r = a*), and the steady–state deviatoric stress is divided by 2. At a distance $r = 3a$, they are divided by 27 and 3, respectively. *Significant deviatoric stresses are present in a much larger rock volume when the steady-state stress distribution is compared to the elastic distribution.*

Second, the deviatoric stress at cavern wall ($r = a$) is divided by *n* when the steady-state stress distribution is compared to the elastic distribution. *Deviatoric stresses in the salt mass are small when the steady-state distribution is reached*. For instance, in a 600-m-deep cavern, $P_\infty - P_c = 6$ MPa; when *n* = 3, the maximum deviatoric stress in the rock mass is 3 MPa. (It is 1.8 MPa when *n* = 5).

It can be inferred from these conclusions that studying the effects of small deviatoric stresses (and slow strain rates) is especially important when assessing cavern steady-state creep closure.

1.4. Pressure solution creep

When fitted against the results of laboratory tests performed in the domain $[0-100°C]\times[5-20\text{MPa}]$, the Norton-Hoff law –- is purely empirical in origin. Extrapolation of the Norton-Hoff law to a range of stresses smaller than the range of stresses against which this law was fitted cannot be substantiated by micro-mechanism analysis.

However, Spiers et al. (1990) observed that pressure-solution creep, an important deformation mechanism in most rocks in the Earth's crust, is especially rapid in rock salt. Theoretical findings strongly suggest that, for this mechanism, the relation between deviatoric stress and strain rate is linear. The strain rate observed during laboratory tests is the sum of the strain rates generated by two mechanisms, dislocation creep and pressure solution creep. At low temperature ($T < 100°C$), dislocation creep is the dominant mechanism in the domain $\sigma > 10$ MPa ; when smaller deviatoric stresses are considered, pressure solution creep usually is dominant. In fact, as underlined by Uraï and Spiers (2007, p.151):

> *"... the relative importance of each process depends strongly on variables such as temperature, confining pressure, grain size, solid solution impurities and second phase content and, importantly, on the presence of sufficient water in grain boundaries to enable solution-precipitation phenomena".)*

According to Uraï and Spiers (2007), the Norton-Hoff (N-H) law typically should be modified in such a way that

$$\dot{\varepsilon} = A\exp\left(-\frac{Q}{RT}\right)\sigma^n + \frac{b}{TD^3}\exp\left(-\frac{\bar{Q}}{RT}\right)\sigma \tag{6}$$

where *b* and $\bar{Q}/R$ are constants, and *D* is the grain diameter. One practical consequence of this is that the creep rate experienced by a salt sample submitted to small deviatoric stresses should be much faster than that extrapolated from the Norton-Hoff law ($b = 0$) fitted on standard laboratory tests (i.e., performed in the range $\sigma =$ 5-20 MPa).

1.5. Laboratory evidence

The effect of small deviatoric stresses (hence, small creep rates — say, $\dot{\varepsilon} < 10^{-10}\,s^{-1}$) have not been investigated widely in the literature, despite their role with regard to geological deformations. Hunsche (1988) performed 10-day long tests during which an axial load of 0.57 MPa was applied on a cylindrical sample; the observed strain rate typically was $7\times10^{-12}\,s^{-1}$. In fact, accurate long-term creep tests are possible only when there is accurate measurement of sample length change (10^{-3}-10^{-2} micrometer), when the applied load remains constant, and, importantly, when the temperature and hygrometry experience very small changes for the duration of the test. Bérest et al. (2005) describe such experiments, performed in deep underground galleries (to take advantage of stable temperature and hygrometry), using extremely accurate sensors and dead-weight loading. They found (Figure 2) that a typical steady-state strain rate when the applied stress was $\sigma = 0.108$ MPa was

$$\dot{\varepsilon} = 1.4\times10^{-12}\ \mathrm{s}^{-1} \tag{7}$$

This rate is exceedingly slow, but it is much faster — by 3 or 4 orders of magnitude —than the creep rate that is extrapolated from tests performed on the same natural rock salt when a deviatoric stress $\sigma = 5-20$ MPa is applied on a sample.

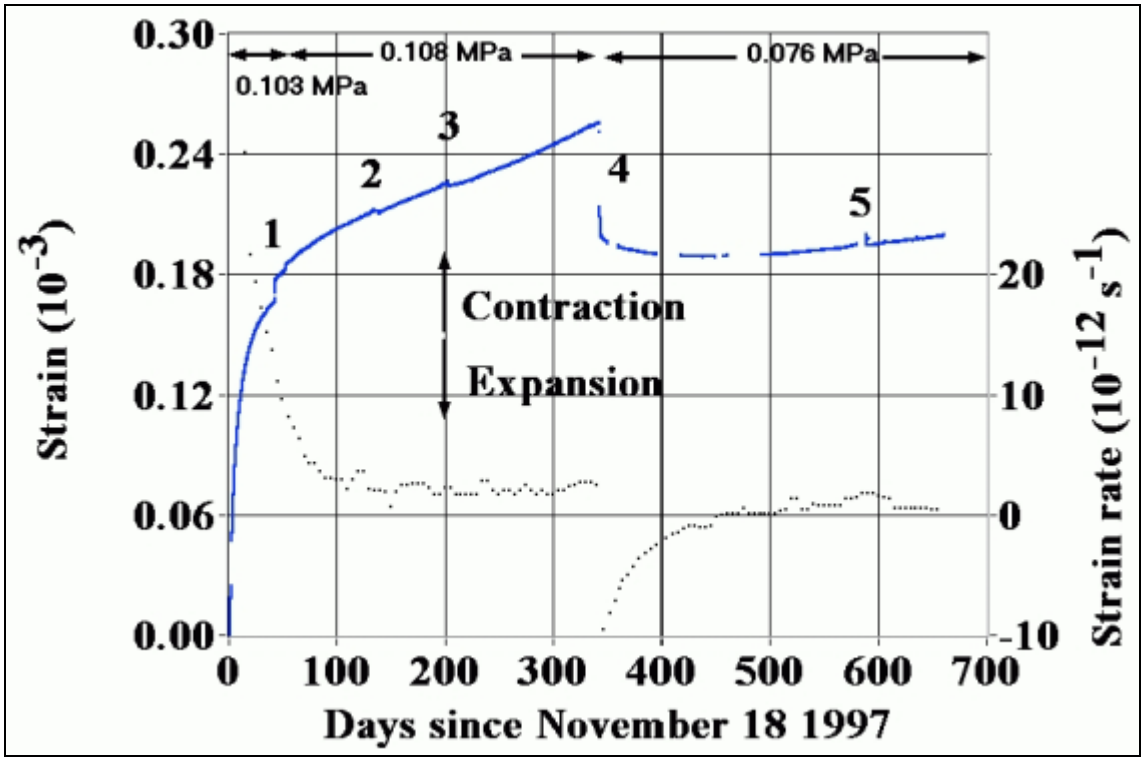

Figure 2. A 22-month-long creep test performed on a salt sample. When the applied stress was 0.108 MPa, the axial creep rate of the was $1.4\times10^{-12}\,s^{-1}$ — a surprisingly fast rate.

1.6. Field evidence

Numerical computations currently are performed to assess the creep closure rates of salt caverns and cavern stability. These computations use constitutive laws that are based on empirical data provided by laboratory tests. In fact, as explained in the following, the deviatoric stresses experienced in a salt mass in the neighborhood of a salt cavern are significantly smaller than the deviatoric stresses applied to salt samples in the laboratory. The constitutive laws fitted against the results of laboratory tests may be irrelevant when predicting the behavior of a salt cavern.

In this context, field evidence could be helpful.

Unfortunately, it is difficult to compare any computational result to the actual behavior of a salt cavern other than in a qualitative manner. Bérest et al. (2006, p.94) observed that:

> *In most cases, it is difficult to measure cavern shape or volume changes directly. In fact, during most mechanical tests, what is measured is the evolution of the wellhead pressure or the flow rate of the expelled [liquid] volume. The evolution of these quantities is influenced not only by purely mechanical effects; factors such as cavern brine warming (or cooling), additional dissolution, brine micro-permeation through the cavern walls and fluid leaks through the casing also play roles. In many cases, for instance, the effects of cavern brine warming are more significant than the effects of cavern creep closure. For this reason, interpreting an in situ "mechanical" test is often difficult.*

In fact, few well-documented *in situ* tests are available. For this reason, monitoring cavern behavior does not provide strong evidence for (or against) any type of governing mechanism in the low-stress range. However, some interesting attempts have been made by Breunesse et al. (2003), who interpreted subsidence data above salt caverns, and by Campos de Orellana (1998),

who examined pillar creep rates in a dry salt mine. A comprehensive discussion of available evidence, both from laboratory experiments and field observations, can be found in Uraï and Spiers (2007).

1.7. Conclusions

The findings at this stage can be summarized as follows.

1. Strong theoretical and experimental evidence supports the view that "pressure solution" plays a significant role, especially when deviatoric stresses are small (say, smaller than $\sigma = 5$ MPa).
2. Simple calculations prove that the cavern closure rate strongly is influenced by phenomena affecting rock salt in the stress domain $\sigma < 5$ MPa .
3. Only few creep tests have been performed on natural salt samples in the range of stress of interest ($\sigma < 5$ MPa).
4. The cavern-creep closure rate might be significantly faster than predicted by the Norton-Hoff law. This is especially true in shallow caverns.
5. *In situ* tests performed on salt caverns are not precise enough to confirm Statement 4.

2. COMPUTATIONS

2.1. A simple "bi-linear" model

The Norton-Hoff, or power, law can be represented in the ($\log\dot{\varepsilon} - \log\sigma$) plane by a straight line with a slope of *n*. This curve correctly fits data in the domain $\sigma = 5 - 20$ MPa , but it widely under-estimates the actual creep rate in the domain $\sigma < 5$ MPa . It is suggested that the mechanical behavior be described by the following bi-linear law:

$$\sigma > S: \qquad \dot{\varepsilon} = A^* \sigma^n \tag{8}$$

$$\sigma < S: \qquad \dot{\varepsilon} = B^* \sigma \tag{9}$$

In other words, when deviatoric stress is large enough, the standard Norton-Hoff law ($n \neq 1$) holds; when deviatoric stress is small, the Newtonian law ($n = 1$) for viscous fluids holds. For continuity, $\dot{\varepsilon}\left(\sigma = S\right) = A^* S^n = B^* S.$

This bi-linear law clearly is simplistic. It would be more realistic to assume that the transition from Dislocation Creep to Pressure Solution is gradual. However, this bi-linear model allows for simple computations. The objective of this paper is to highlight the significance of small deviatoric stresses; precise prediction will be possible when the database is larger.

Consider an idealized spherical cavern and steady-state creep closure: when the cavern is deep enough, the rock mass is divided in two zones. In the zone closest to the cavern, deviatoric stresses are large, and (8) holds. Farther from the cavern, deviatoric stresses are small, and (9) holds. The steady-state cavern closure rate can be computed easily (Appendix A):

$$\left.\frac{\dot{V}}{V}\right|_{SS}^{BL} = -\frac{3}{2} A \left\{ \frac{3}{2n} \left[P_\infty - P_c + \frac{2}{3}(n-1) S \right] \right\}^n = \left[1 + \frac{2(n-1)S}{3(P_\infty - P_c)} \right]^n \times \left.\frac{\dot{V}}{V}\right|_{SS}^{NH} \tag{10}$$

For instance, n = 3, S = 1.5 MPa, $P_\infty - P_c$ = 10 MPa and $\left.\frac{\dot{V}}{V}\right|_{SS}^{BL} = 1.7 \left.\frac{\dot{V}}{V}\right|_{SS}^{NH}$. Even when "reasonable" values of n and S are selected, the creep closure rate is significantly faster when the Norton-Hoff creep law is modified slightly to take into account the effect of small deviatoric stresses.

The case in which S = 1.5 MPa is discussed in more detail on Figures 3, 4 and 5.

The bi-linear law is drawn on Figure 3, which represents the decimal logarithm of the stress (σ, in MPa) applied on the sample versus the decimal logarithm of the axial strain rate ($\dot{\varepsilon}$, in s^{-1} or yr^{-1}). When the applied stress is smaller than $S = 1.5$ MPa, salt behavior is governed by (9). When the applied stress is larger than $S = 1.5$ MPa, salt behavior is governed by (8); several values of the stress exponent (n) of the Norton-Hoff (power) law are considered, n = 1 to 5.

On Figure 4, the decimal logarithm of the difference between geostatic pressure and cavern pressure, ($P_\infty - P_c$, in MPa, which is related simply to cavern depth through H [in meters] = 0.01 ($P_\infty - P_c$).), is plotted versus cavern steady-state closure rate ($-\dot{V}/V$, in s^{-1} or yr^{-1}) for various values of the exponent n of the power law.

On Figure 5, the decimal logarithm of cavern closure rate ($-\dot{V}/V$) is plotted against the decimal logarithm of the difference between geostatic pressure and cavern pressure ($P_\infty - P_c$) in the case S = 1.5 MPa. The Norton-Hoff (N-H) constitutive law and the bi-linear (B-L) constitutive law are considered. The ratio between the N-H creep closure rate and the B-L creep closure rate is $\left.\frac{\dot{V}}{V}\right|_{SS}^{BL} \Big/ \left.\frac{\dot{V}}{V}\right|_{SS}^{NH} = 1.7$, when the cavern is 1000-m deep (or $P_\infty - P_c = 10$ MPa). It is $\left.\frac{\dot{V}}{V}\right|_{SS}^{BL} \Big/ \left.\frac{\dot{V}}{V}\right|_{SS}^{NH} = 8$, when the cavern is 200-m deep (or $P_\infty - P_c = 2$ MPa): the difference between the two constitutive laws is strengthened when shallow caverns are considered.

In this example, the threshold separating the two creep mechanisms is S = 1.5 MPa. This figure was selected as an example: at this time, there is insufficient information to substantiate such a choice. Figures 6, 7 and 8 correspond to the case S = 3 MPa.

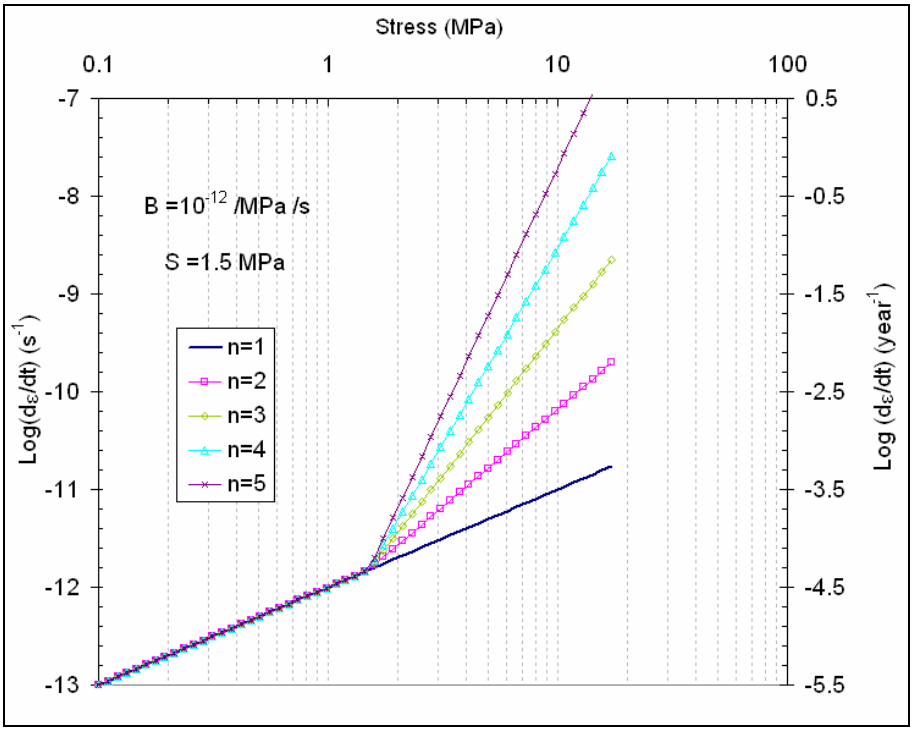

Figure 3. The bi-linear creep model, *S* = 1.5 MPa. Various values of the power-law stress exponent are considered.

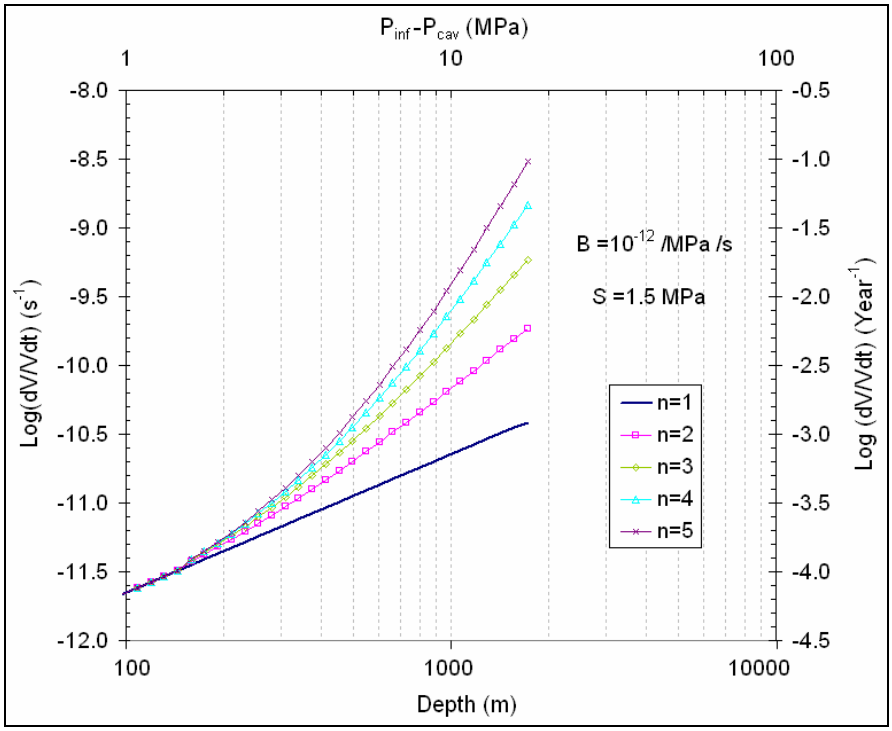

Figure 4. Cavern convergence rate versus cavern depth when the bi-linear creep model is considered.

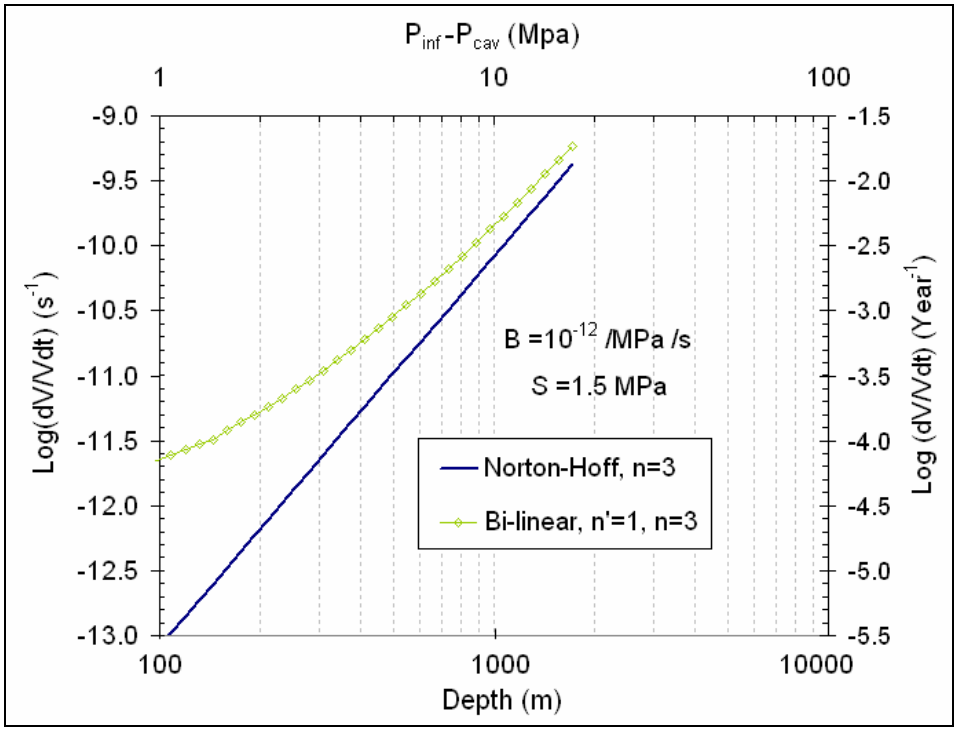

Figure 5. Cavern-creep closure rate: Comparison between the Norton-Hoff and the bi-linear laws.

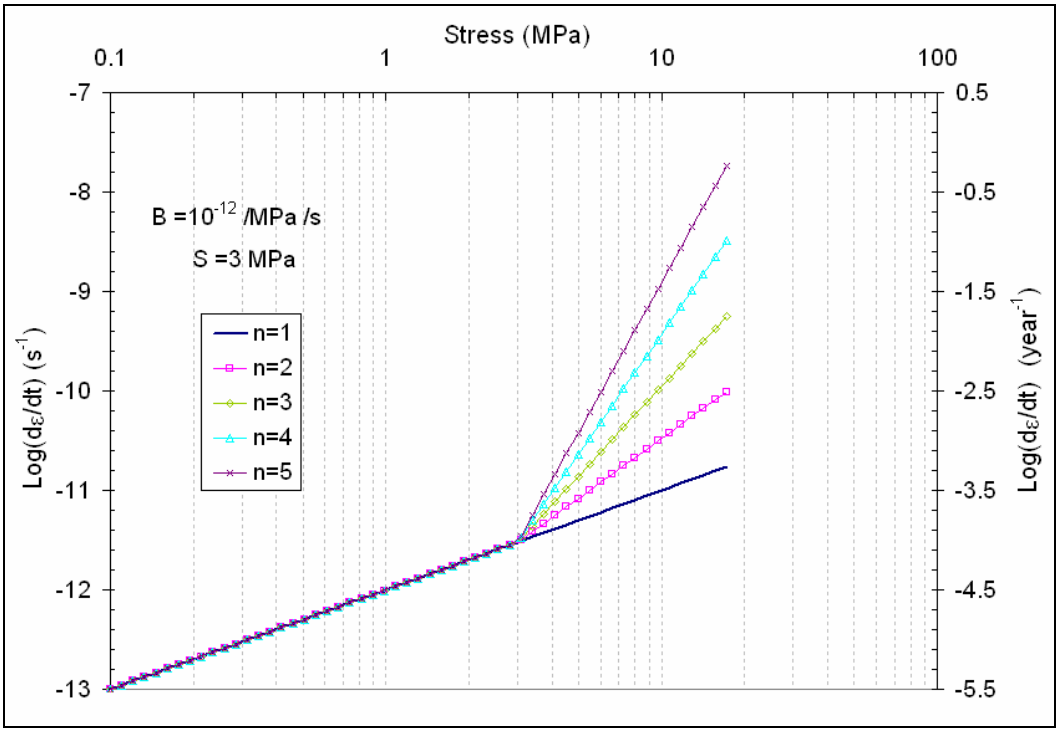

Figure 6. The bi-linear creep model, *S* = 3 MPa.

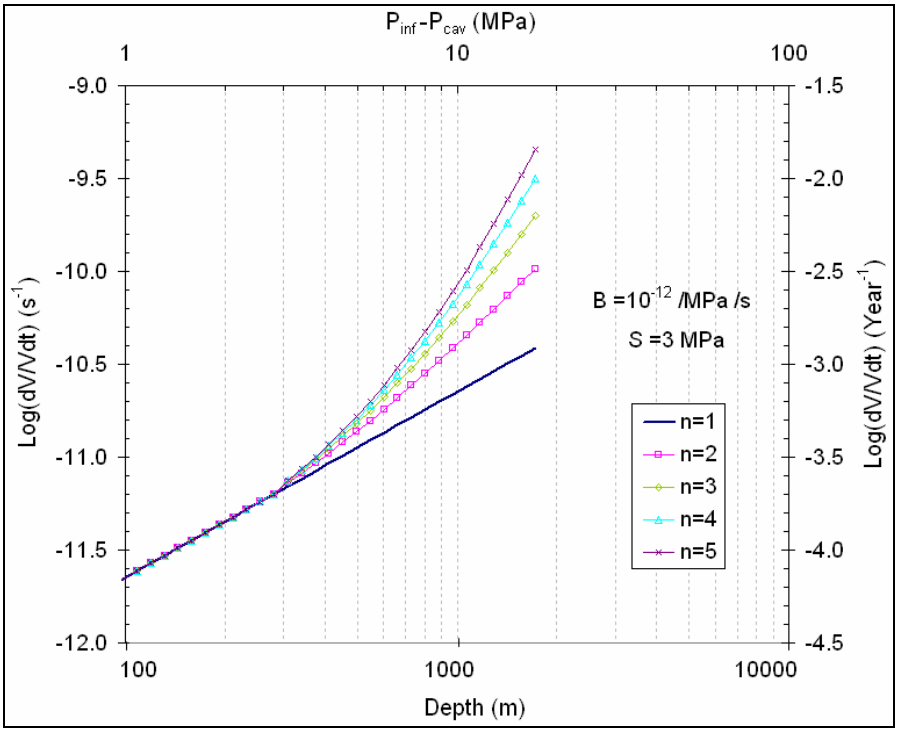

Figure 7. Cavern convergence rate versus cavern depth when the bi-linear creep model is considered, *S* = 3 MPa.

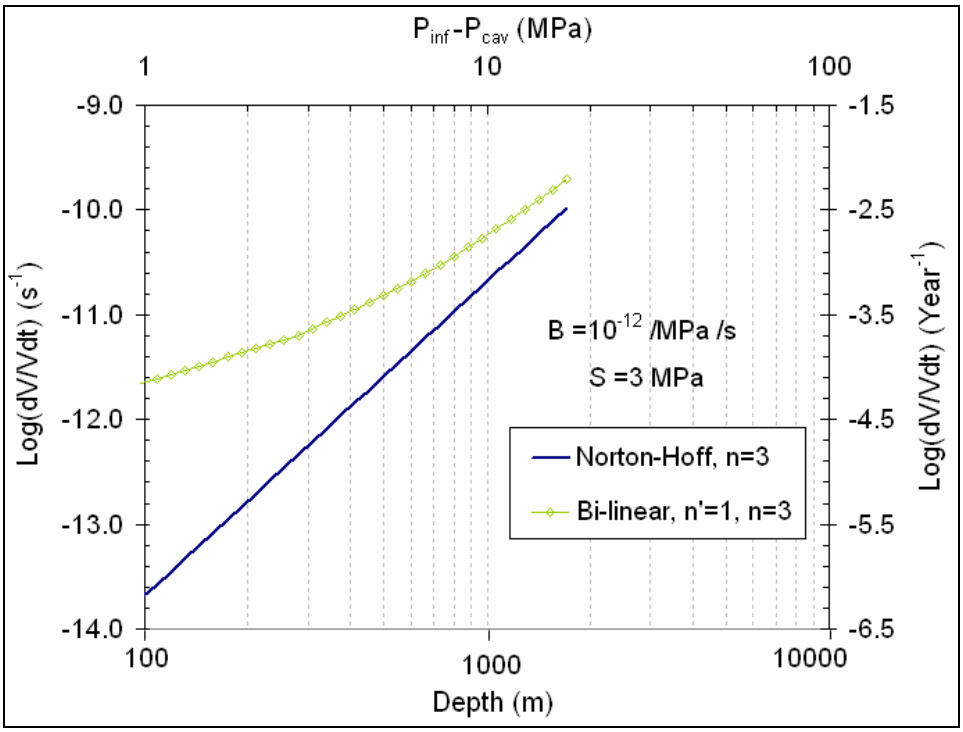

Figure 8. Cavern creep closure rate: comparison between the Norton-Hoff and the bi-linear laws, *S* = 3 MPa.

2.2. Numerical computations

Numerical computations also were performed using LOCAS (Brouard et al., 1996). For these computations, a more realistic cavern shape was considered. EZ53, a 8000-m^3 cavern at the Gaz de France Etrez storage site was selected. Its actual depth is 950 m, but the influence of depth was discussed and, computations were performed considering different depths (Figure 9): $H = 950$ m (Figure 10); $H = 600$ m (Figure 11); and $H = 250$ m (Figure 12). The Norton-Hoff parameters were $n = 3.1$ and $A^* = 10^{-13}/\text{MPa}^{3.1}\text{-s}$. (The effect of temperature on creep rate was not considered.) Parameters of the bi-linear law were S = 3 MPa and $B^* = 10^{-12}/\text{MPa-s}$.

When the cavern depth is $H = 950$ m, the difference between the Norton-Hoff law and the bi-linear law is small — and probably undetectable through *in situ* tests. When the cavern is shallow, differences are more pronounced. When cavern depth is $H = 250$ m, the Norton-Hoff law predicts that the relative cavern closure rate is $\dot{V}/V = 5\times10^{-4}/\text{yr}$; it is $\dot{V}/V = 10^{-4}/\text{yr}$ when the bi-linear law is used.

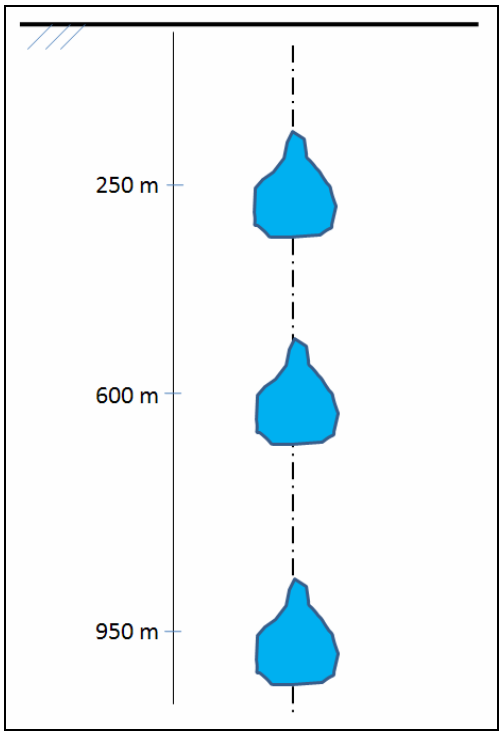

Figure 9. Numerical computations were performed at three cavern depths.

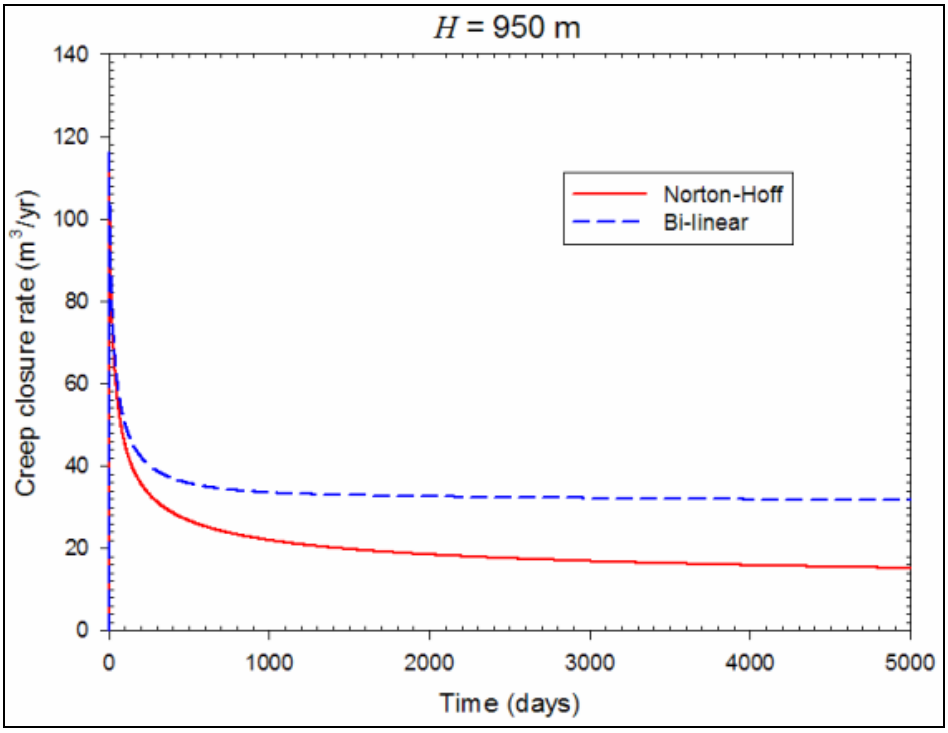

Figure 10. Cavern depth is 950 m.

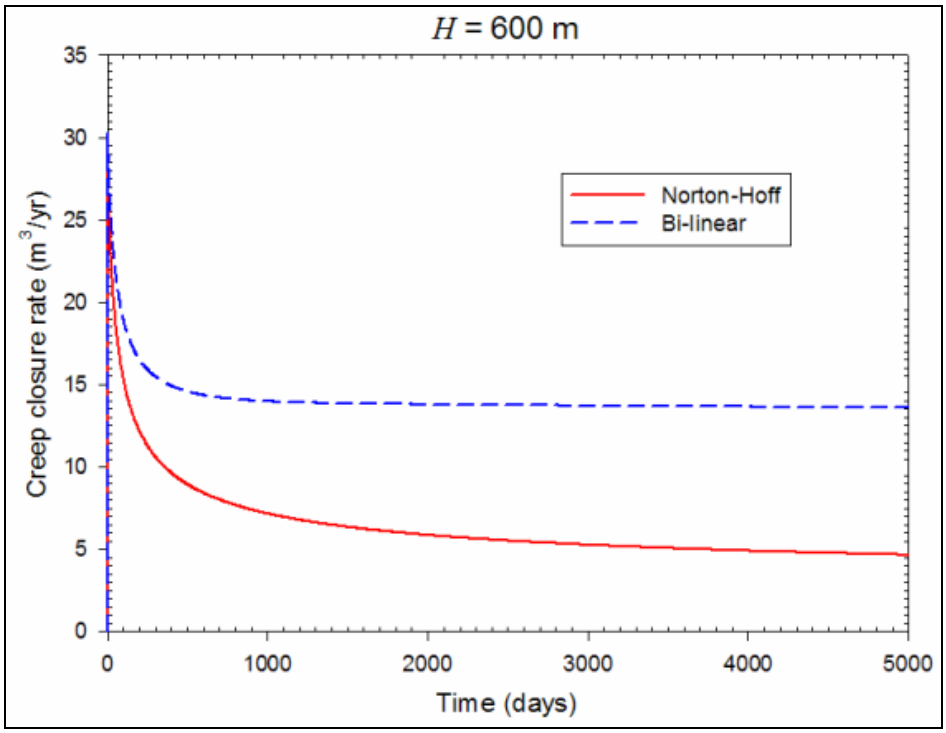

Figure 11. Cavern depth is 600 m.

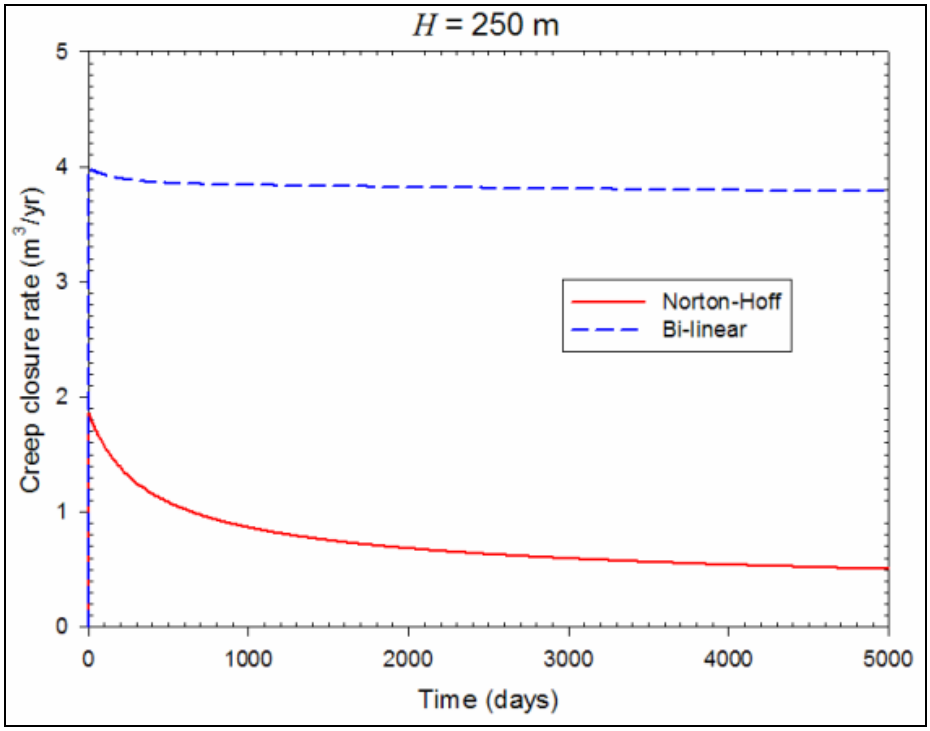

Figure 12 – Cavern depth is 250 m.

REFERENCES

Bérest P., Blum P.A., Charpentier J.P., Gharbi H. and Valès F. (2005) Very slow creep tests on rock samples. International Journal of Rock Mechanics and Mining Sciences 42, 569-576.

Bérest P., Karimi-Jafari M., Brouard B. and Bazargan B. (2006) In Situ Mechanical Tests in Salt Caverns. Proc. SMRI Spring Meeting, Brussels, 91-129.

Blum W. and Fleischmann C. (1988) On the deformation-mechanism map of rock salt. *Proc. 2nd. Conf. Mech. Beh. of Salt.* Clausthal-Zellerfeld, Germany: Transactions of Technical Publishers, 7-23.

Breunesse J.N., van Eijs R.M.H.E, deMeer S. and Kroon I.C. (2003) Observation and prediction of the relation between salt creep and land subsidence in solution-mining-The Barradeel case. Proc. SMRI Fall Meeting Chester, 38-57.

Brouard B., Karimi-Jafari, M., Bérest P. and Frangi A. (2006) Using LOCAS Software to Better Understand the Behavior of Salt Caverns. Proc. SMRI Spring Meeting, Brussels, 273-288.

Campos de Orellana A.J. (1998). Non-Associated Pressure Solution Creep in Salt Rock Mines. *Proc. 4th Conf. Mech. Beh. of Salt,* Transactions of Technical Publishers, 429-444.

Hunsche U. (1984) Results and interpretation of creep experiments on rock salt. *Proc. 1st Conf. Mech. Beh. of Salt.* Clausthal-Zellerfeld, Germany: Transactions of Technical Publishers, 159-167.

Hunsche U. (1988). Measurement of creep in rock salt at small strain rates. *Proc. 2nd Conf. Mech. Beh. of Salt* Clausthal-Zellerfeld, Germany: Transactions of Technical Publishers, 187-196.

Langer M. (1984).The rheological behaviour of rock salt. *Proc. 1st Conf. Mech. Beh. of Salt.* Clausthal-Zellerfeld, Germany: Transactions of Technical Publishers, 201-240.

Munson D.E. and Dawson P.R.(1984) Salt constitutive modeling using mechanism maps. *Proc. 1st Conf. Mech. Beh. of Salt.* Clausthal-Zellerfeld, Germany: Transactions of Technical Publishers, 717-737.

Schléder Z. and Uraï J.L.(2005). Microstructural evolution of deformation-modified primary Halite from Hengelo, the Netherlands. International Journal of Earth sciences, 94(5-6): 941-956.

Spiers C.J., Schutjens P.M.T.M., Brzesowsky R.H., Paech C.J., Liezenberg J.L. and Zwart H.J. (1990). Experimental determination of the constitutive parameters governing creep of rocksalt by pressure solution. In: Knipe R.J. and Rutter E.H.(eds) deformation Mechanisms, Rheology and Tectonics. Geological Society special Publication 54: 215-227.

Uraï J.L. and Spiers C.J. (2007). The effect of grain boundary water on deformation mechanisms and rheology of rocksalt during long-term deformation. *Proc. 6th Conf. Mech. Beh. of Salt*, Taylor & Francis Group, 149-158.

APPENDIX A — CONSTITUTIVE EQUATIONS

In the following we consider a spherical cavern of radius *a*, leached out from an infinite viscoplastic medium. Spherical symmetry is assumed. Steady-state has been reached. When the cavern is deep enough ($P_\infty - P_c > 2S/3$), the rock mass is divided in two zones. In the zone closest to the cavern, or $r < x$, deviatoric stresses are large, or $\sqrt{3J_2} > S$. Farther from the cavern, or $r > x$, deviatoric stresses are small, and $\sqrt{3J_2} < S$. The mechanical constitutive law can be written as

$$\dot{\varepsilon}_{ij} = \frac{1+\nu}{E}\dot{\sigma}_{ij} - \frac{\nu}{E}\dot{\sigma}_{kk}\delta_{ij} + \frac{3}{2}A^*(\sqrt{3J_2})^{n-1}s_{ij} \text{ when } \sqrt{3J_2} > S \text{, or } r < x$$

$$\dot{\varepsilon}_{ij} = \frac{1+\nu}{E}\dot{\sigma}_{ij} - \frac{\nu}{E}\dot{\sigma}_{kk}\delta_{ij} + \frac{3}{2}B^*s_{ij} \text{ when } \sqrt{3J_2} < S \text{, or } r > x$$

Continuity implies $A^*S^n = B^*S$.

The equilibrium equation can be written $\sigma_r - \sigma_\theta = -\frac{r}{2}\frac{\partial\sigma_r}{\partial r}$,

and the boundary conditions are

$$\sigma_{rr}(a, t<0) = -P_\infty$$

$$\sigma_{rr}(a, t>0) = -P_c$$

$$\sigma_{rr}(\infty) = -P_\infty$$

$u = u(r)$ is the radial displacement when spherical symmetry is taken into account:

- When $\sqrt{3J_2} > S$:

$$\dot{\varepsilon}_{rr} = \frac{\partial \dot{u}}{\partial r} = \frac{1}{E}\left(\dot{\sigma}_{rr} - 2\nu\dot{\sigma}_{\theta\theta}\right) + A^*\left(\sigma_{rr} - \sigma_{\theta\theta}\right)^n \tag{11}$$

$$\dot{\varepsilon}_{\theta\theta} = \dot{\varepsilon}_{\varphi\varphi} = \frac{\dot{u}}{r} = \frac{1}{E}\left[\left(1-\nu\right)\dot{\sigma}_{\theta\theta} - \nu\dot{\sigma}_{rr}\right] - \frac{A^*}{2}\left(\sigma_{rr} - \sigma_{\theta\theta}\right)^n \tag{12}$$

- When $\sqrt{3J_2} < S$:

$$\dot{\varepsilon}_{rr} = \frac{\partial \dot{u}}{\partial r} = \frac{1}{E}\left(\dot{\sigma}_{rr} - 2\nu\dot{\sigma}_{\theta\theta}\right) + B^*\left(\sigma_{rr} - \sigma_{\theta\theta}\right) \tag{13}$$

$$\dot{\varepsilon}_{\theta\theta} = \dot{\varepsilon}_{\varphi\varphi} = \frac{\dot{u}}{r} = \frac{1}{E}\left[\left(1-\nu\right)\dot{\sigma}_{\theta\theta} - \nu\dot{\sigma}_{rr}\right] - \frac{B^*}{2}\left(\sigma_{rr} - \sigma_{\theta\theta}\right) \tag{14}$$When a steady-state solution is reach

$$\frac{\partial \dot{u}}{\partial r} + 2\frac{\dot{u}}{r} = 0$$

from which $\dot{u} = a^2\dot{a}/r^2$ can be inferred. (12) can be rewritten as

$$\frac{a^2\dot{a}}{r^3} = -\frac{A^*}{2}\left(-\frac{r}{2}\frac{\partial\sigma_r}{\partial r}\right)^n \text{ when } \sqrt{3J_2} > S$$

$$\frac{a^2\dot{a}}{r^3} = -\frac{B^*}{2}\left(-\frac{r}{2}\frac{\partial\sigma_r}{\partial r}\right) \text{ when } \sqrt{3J_2} < S$$

The first equation holds when $r < x$; the second equation holds when $r > x$.

These two equations can be integrated with respect to r in the $[a,x]$ domain and in the $[x,\infty]$ domain; from the second equation, it can be inferred that $\sigma_{rr}(x) = -P_\infty + 2S/3$ and

$$\left.\frac{\dot{V}}{V}\right|_{t=\infty} = 3\left.\frac{\dot{a}}{a}\right|_{t=\infty} = -\frac{3}{2}A\left\{\frac{3}{2n}\left[P_\infty - P_c + \frac{2}{3}(n-1)S\right]\right\}^n$$